Solar-wind influence on MLT dependence of plasma sheet conditions and their effects on storm time ring current formation

Margaret W. Chen,[1] Chih-Ping Wang,[2] Michael Schulz,[3] and Larry R. Lyons[2]

Received 28 March 2007; revised 18 May 2007; accepted 6 June 2007; published 27 July 2007.

[1] By applying plasma sheet boundary conditions based on averages of Geotail data to a magnetically self-consistent ring current simulation model, we investigate how solar-wind influence on plasma sheet conditions affects local-time asymmetries in early ring current development under two representative interplanetary conditions: (1) For strongly northward interplanetary magnetic field (IMF), high solar-wind density, and low solar-wind speed, Geotail ion densities are high and ion temperatures are low, particularly in the post-midnight quadrant at radial distances $r > 8\ R_E$; and (2) For weakly northward IMF, high solar-wind speed, and low solar-wind density, a significant density enhancement is not observed in the post-midnight at $r > 8\ R_E$. Within an hour after an increase in the convection electric field, Condition (1) lead to relative enhancement of the simulated ring current plasma pressure especially in the post-midnight quadrant, while Condition (2) lead to pressure enhancements that are more uniformly distributed around the night side. **Citation:** Chen, M., C.-P. Wang, M. Schulz, and L. R. Lyons (2007), Solar-wind influence on MLT dependence of plasma sheet conditions and their effects on storm time ring current formation, *Geophys. Res. Lett.*, *34*, L14112, doi:10.1029/2007GL030189.

1. Introduction

[2] It is known that the plasma sheet depends on interplanetary conditions. For example, *Borovsky et al.* [1997] reported a strong correlation between the solar-wind ion density and the plasma sheet ion density in the magnetotail. They found that a "superdense" plasma sheet (in which the plasma sheet density was several times higher than its average value) occurred when *Kp* rose after it had been low for an extended period. Cold dense plasma has been reported to be present at dawn in the plasma sheet during active times [*Denton et al.*, 2005; *Lavraud et al.*, 2005]. Such cold dense plasma sheet material could then be delivered into the inner magnetosphere either by a sudden southward turning of the IMF or by a very strong magnetospheric compression caused by a large increase in the solar wind dynamic pressure following an extended interval of northward IMF or very weak IMF B_z [*Thomsen et al.*, 2003]. Several drift-loss simulation studies have shown that a superdense plasma sheet can lead to a strong ring current [e.g., *Chen et al.*, 1994; *Kozyra et al.*, 1998; *Ebihara and Ejiri*, 2000; *Liemohn et al.*, 2001].

[3] The dependence of the nightside plasma sheet ion density and temperature distributions and in particular their local time asymmetries on interplanetary conditions have been examined recently by C.-P. Wang et al. (Sources, transport, and distributions of plasma sheet ions and electrons and dependences on interplanetary parameters under northward interplanetary magnetic field, submitted to *Journal of Geophysical Research*, 2007, hereinafter referred to as Wang et al., submitted manuscript, 2007). They binned Geotail data in the nightside plasma sheet (plasma $\beta > 1$, between $r = 8\ R_E$ and $X_{GSM} = -30\ R_E$) from January 1995 through December 2005 for ions with energies of 21 eV/q to 3000 keV/q according to 8 specified interplanetary conditions that are a combination of three interplanetary parameters in their low or high value range: low solar-wind density (<6.5 cm^{-3}), high solar-wind density (6.5 to 15 cm^{-3}), low solar-wind speed (<400 km/s), high solar-wind speed (400 to 1000 km/s) for weakly northward IMF B_z (0–2 nT) and for strongly northward IMF B_z (2–8 nT). Wang et al. (submitted manuscript, 2007) then time-averaged the measured local ion densities and temperatures over those separate portions of the Geotail database that corresponded to each of the specified interplanetary conditions. For the present study we selected two of these eight conditions because they had the overall highest density and temperature, respectively.

[4] Condition 1. For strongly northward IMF, high solar-wind density, and low solar-wind speed, the overall ion density was the highest among the northward IMF conditions and there was a strong dawn-dusk asymmetry at radial distances $r > 8\ R_E$ (with the highest density in the post-midnight quadrant). The high densities there were associated with low ion temperatures. This is illustrated in Figures 1a and 1b, which display Geotail average equatorial plasma sheet ion density and temperature, respectively.

[5] Condition 2. For weakly northward IMF, high solar-wind speed, and low solar-wind density, the overall ion density is the lowest and the temperature was highest among all the northward IMF conditions considered, and there was no strong density enhancement in the post-midnight quadrant at $r \sim 8\ R_E$, such as was seen in Condition (1). The lower ion densities and higher ion temperatures characteristic of Condition (2) are illustrated in Figures 1c and 1d, respectively.

[6] Because these two conditions represented the relatively extreme (in density and temperature) among the eight cases, we expected to find the most differences between these conditions.

[1] Aerospace Corporation, El Segundo, California, USA.
[2] Department of Atmospheric and Oceanic Sciences, University of California, Los Angeles, California, USA.
[3] Lockheed Martin Advanced Technology Center, Palo Alto, California, USA.

0094-8276/07/2007GL030189

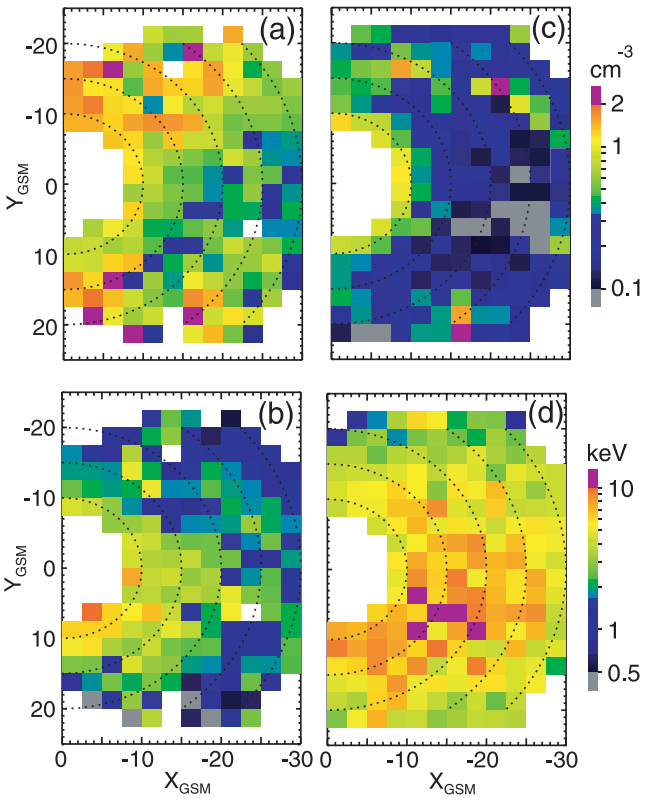

Figure 1. Time-averaged Geotail ion density and temperature in the equatorial plasma sheet under Conditions (a, b) 1 and (c, d) 2.

[7] The particle transport is a superposition of mostly azimuthal gradient-curvature drift that is proportional to the particle energy and the mostly sunward $\mathbf{E} \times \mathbf{B}$ drift which is independent of particle energy. Thus, for particles of ring current energies, those with low-energy tend to penetrate deeper in L under the influence of the $\mathbf{E} \times \mathbf{B}$ drift. We therefore expect that Condition (1), in which there is a population of mostly lower-energy ions in the post-midnight quadrant, should lead to a relatively stronger enhancement of ring current pressure in the post midnight sector, whereas Condition (2), in which there is a population of mostly high-energy particles in the pre-midnight sector, should lead to a relatively weaker enhancement of ring current pressure in the pre-midnight quadrant. In the interest of investigating the local-time effects of plasma sheet preconditioning on formation of the storm time ring current, we test these hypotheses by carrying out magnetically self-consistent simulations of the ring current with the appropriate boundary conditions that correspond to the two selected representative conditions. We focus on the first few hours of the storm development because it best reveals the effects of plasma sheet preconditioning on ring current formation. *Lavraud et al.* [2006] suggested that the onset of enhanced convection that transports plasma sheet particles to form the ring current also leads to magnetic reconnection in the midtail that can lead to removal of the plasma sheet located tailward of the reconnection line. Thus, new plasma with significantly different properties is supplied to the plasma sheet shortly after a southward turning of the IMF.

2. Plasma Sheet Boundary Conditions to Ring Current Simulation Model

[8] We use a drift-loss ring current simulation model in which we impose magnetic self-consistency in the equatorial plane. We summarize our model only briefly here, since it is described in detail elsewhere [*Liu et al.*, 2006; *Chen et al.*, 2006]. The guiding-center drifts of equatorially-mirroring protons and electrons that conserve their first invariants M are traced in a model of the magnetic and electric fields. The magnetic field lines in this model are described semi-analytically with a parameter that stretches each field line (L, φ) relative to a dipolar model, by an amount that depends on its equatorial radius r_0 and its longitude φ. We assume for simplicity that the field lines lie in meridian planes. The equatorial magnetic intensity B_0 at a given r_0 and φ, found by solving the force balance equation, determines the stretching parameter for each field line. The electrostatic potential includes corotation, quiescent *Volland* [1973]-*Stern* [1974] convection, and a less well-shielded storm time enhancement in convection that penetrates to lower L values. Our imposed electrostatic field is not currently self-consistent. For this study we assume that the cross-polar cap potential increases slowly from its quiescent value of 25 kV to 37.5 kV during the first hour and then rises more rapidly to 118 kV over the next hour. This was chosen to represent the early rise of the cross-polar cap potential during the main phase of a moderate storm. We simulated only the first two hours of the storm to focus on the effects of plasma sheet preconditioning.

[9] Using the drift trajectories, initial conditions and boundary conditions, we map phase space densities f taking account of loss: charge exchange for protons; weak diffusion inside the plasmasphere [*Albert*, 1994] and scattering due to electron cyclotron harmonic waves outside the plasmasphere [*Lyons*, 1974] for electrons. The ring current's perpendicular pressure is calculated from f. Then the force-balance equation is solved to update the magnetic intensity every 20 minutes of simulated time. The initial conditions are taken from solutions to the proton and electron steady-state transport equations. The time-dependent boundary conditions, applied at geosynchronous altitude (r_0 = 6.6 R_E), are based on the MLT and Kp-binned averaged LANL/MPA data of *Korth et al.* [1999] for electrons. For protons, the dynamic boundary conditions are taken (respectively) from the time-averaged Geotail data for the two separate interplanetary conditions described in Section 1 and updated every 20 minutes in the simulation. Since the lowest radial distance of the Geotail data is at $\approx 8\ R_E$, we need to map the data to geosynchronous altitude, the present outer boundary of the ring current simulation model. We used a modified version [*Wang et al.*, 2003] of the Rice University Magnetospheric Specification Model (MSM) [*Freeman et al.*, 1993] and the *Tsyganenko* [1996] (T96) magnetic field model to specify time-dependent magnetic and electric fields. For a given r_0 and φ we mapped the Geotail ion flux at each kinetic energy to the number of ions per unit flux tube for the corresponding "energy" invariant

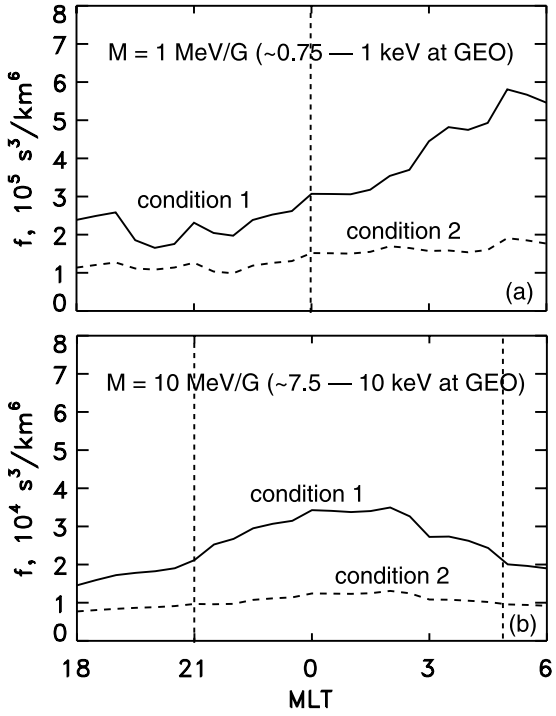

Figure 2. Phase space density f versus MLT on the night side at geosynchronous altitude for ions having (a) M = 1 MeV/G and (b) M = 10 MeV/G.

λ of an isotropic distribution [*Wolf*, 1983]. Varying the cross-tail potential drop as described earlier, we traced the electric and magnetic drift of ions of different energy λ values within the MSM and T96 models. We obtained the phase space density at geosynchronous altitude for the time-averaged Geotail ion fluxes corresponding (respectively) to the two interplanetary conditions described earlier. We applied these time-dependent phase space distributions as the proton boundary conditions on the ring current simulation model.

[10] Figure 2 shows two examples of the simulated phase space density distribution on the night side at $t = 0$ for ions having a first invariant value of 1 MeV/G (~0.75–1 keV at $r_0 = 6.6\ R_E$) (Figure 2a) and 10 MeV/G (~7.5–10 keV at $r_0 = 6.6\ R_E$) (Figure 2b). The solid curve corresponds to Condition 1 (the strongly northward IMF case) and the dashed curve corresponds to Condition 2 (the weakly northward IMF case). The phase space density turns out to be larger for Condition 1 than for Condition 2 along the night side for the indicated M values. The phase space density is especially higher for Condition 1 than for Condition 2 in the post-midnight quadrant for low M values (0.5 MeV/G $\leq M \leq$ 6 MeV/G), as shown by the example in Figure 2a. For high M (6 MeV/G $\leq M \leq$ 40 MeV/G), the enhancement of f for Condition 1 is centered roughly at 01:00 MLT (see Figure 2b). Ions with the lower M values or energies tend to be transported deeper into the inner magnetosphere during enhanced convection because their $\mathbf{E} \times \mathbf{B}$ drift is more likely to dominate over their gradient drift. Thus, we expect that plasma sheet ions associated with Condition 1 (being of lower energy on average than those associated with Condition 2) would be preferentially transported to lower L values within the post-midnight quadrant shortly after a southward turning of the IMF.

3. Simulation Results

[11] We present results of two simulations of the ring current using dynamic boundary conditions based on mapped Geotail data for Conditions 1 (strongly northward IMF; cold dense plasma sheet) and 2 (weakly northward IMF; hot tenuous plasma sheet), respectively. The purpose here is to simulate the formation of the ring current associated with enhanced convection following the two different representative interplanetary conditions. Figure 3 shows the simulated perpendicular pressure in the equatorial plane at different simulation times for Condition 1 (Figures 3a, 3b, 3c, and 3d) and Condition 2 (Figures 3e, 3f, 3g, and 3h). We compare the results, noting differences especially in local time asymmetries. Overall, the perpendicular pressure on the night side tends to be larger for Condition 1 than for Condition 2. This is consistent with the findings of *Lavraud and Jordanova* [2007] that (for the same plasma sheet pressure) a cold dense plasma sheet leads to a stronger storm time ring current than does a hot tenuous plasma sheet. This is because low-energy ions are preferentially

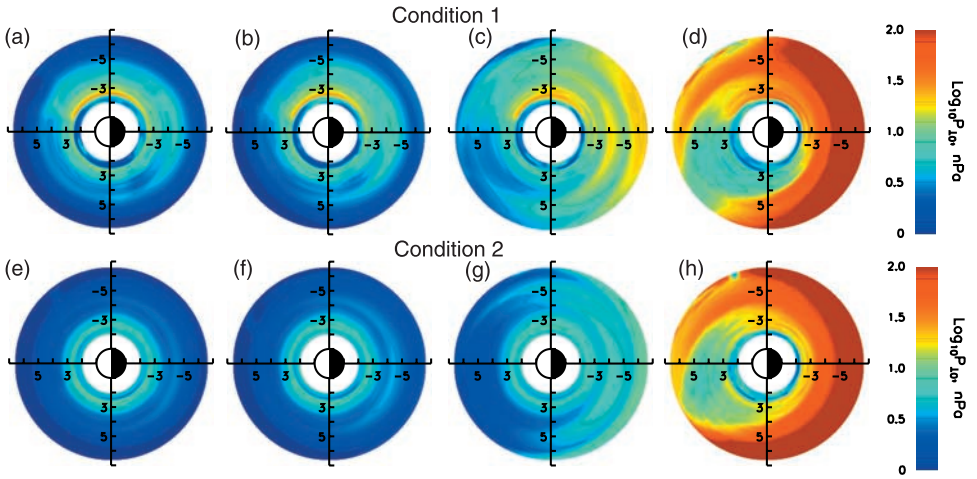

Figure 3. Simulated equatorial perpendicular pressure for Conditions 1 and 2 at (a, e) $t = 0.33$ hr, (b, f) $t = 0.67$ hr, (c, g) $t = 1.33$ hr, and (d, h) $t = 2$ hr.

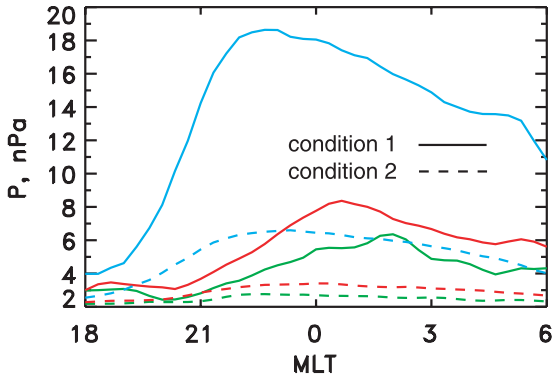

Figure 4. Equatorial perpendicular pressure versus MLT on the night side for Conditions 1 (solid curves) and 2 (dashed curves). Green, red, and blue curves correspond to $t = 0.33$ hr, 0.67 hr, and 1.33 hr, respectively.

transported to lower L values. Thus, a dense population of low-energy ions is more effective than a population of higher-energy (higher temperature) ions in contributing to a strong ring current. During the first 40 minutes into the simulation, the perpendicular pressure was enhanced substantially more in the post midnight (morning) quadrant for Condition 1 (the two conditions are described in the beginning of the paragraph) than for Condition 2. These results confirm our earlier hypothesis that there would be a more enhanced ring current in the post-midnight quadrant early during a storm that follows Condition 1 based on the corresponding characteristics of the plasma sheet boundary conditions. By simulation time t = 1.33 hr the polar cap potential had been significantly enhanced and the perpendicular pressure for Condition 1 was more uniformly distributed around the night side, as was the perpendicular pressure for Condition 2. Reasons for this are twofold: (1) the plasma sheet boundary conditions have evolved and there is less preferential enhancement of plasma sheet ions in the post-midnight quadrant after the IMF is no longer northward; (2) ions that had been transported rapidly to the post-midnight quadrant have gradient-drifted westward. However, even at t = 2 hr, there were still differences in the perpendicular pressure distributions for the two cases; the most notable being that the larger pressures occurred at lower radial distances from about 2100 MLT to 0500 MLT on the night side for Condition 1 than for Condition 2.

[12] The longitudinal distribution of the equatorial perpendicular pressure at $r_0 = 4.2\ R_E$ for the two runs, shown in Figure 4, more clearly illustrate differences between Conditions 1 (solid curve) and 2 (dashed curve). At $t = 0.33$ hr, the perpendicular pressure for Condition 1 peaked in the post-midnight quadrant. As time progressed the pressure became enhanced more broadly from pre-midnight to dawn for Condition 1 as for Condition 2. Thus, it was early on in the simulated storm that the ring current pressure tended to be preferentially enhanced in the post-midnight quadrant following a strongly northward IMF condition (corresponding to a cold dense plasma sheet).

4. Conclusions

[13] In this study we investigated the local-time effects of plasma sheet preconditioning on the early formation of the storm time ring current. We focused on the first two hours of storm development because new plasma with significantly different properties is supplied to the plasma sheet shortly after a southward turning of IMF [*Lavraud et al.*, 2006]. Two representative realistic northward IMF plasma sheet conditions (based on Geotail observations) were considered: (1) cold and dense particularly in the post-midnight sector and (2) hot and tenuous. These conditions were selected because they had the highest plasma sheet density and temperature, respectively, among the cases that we considered. Our magnetically self-consistent ring current simulations supports the hypothesis that Condition (1) would lead to relative enhancement of the ring current plasma pressure in the post-midnight quadrant, whereas Condition (2) would lead to smaller pressure enhancements that are more uniformly distributed around the night side shortly after an increase of the convection electric field. This is because lower-energy ions are able to be transported farther inward than the higher-energy ions by $\mathbf{E} \times \mathbf{B}$ drift, which must compete with the transport-inhibiting effects of gradient-curvature drift. A cold dense plasma sheet (associated with strongly northward IMF, high solar-wind density and low solar-wind speed) is thus more effective than a hot tenuous plasma sheet (associated with weakly northward IMF, high solar-wind speed and low solar-wind density) in building up a ring current under the influence of the same enhanced convection electric field. Our simulations illustrate consequences for representative plasma sheet conditions under northward IMF [cf. *Denton et al.*, 2005; *Lavraud et al.*, 2005]; results would vary for individual storms. However, our study clearly shows the importance of plasma sheet preconditioning on the local time development of the storm-time ring current especially during the first few hours of the main phase. Our study also further confirms that realistic models of the ring current require realistic empirical and/or numerical models of the plasma sheet.

[14] **Acknowledgments.** The work of M. W. Chen was supported in part by NSF grants NSF-ATM-0548715 and NSF-ATM-062708, NASA grant NNX06AC39G, and by The Aerospace Corporation's Independent Research Development Program. The work at UCLA was supported in part by NSF grant ATM-0207298. The work of M. Schulz was supported by NSF Grant ATM-0548915 and NASA Grant NNX06AC39G. Computing resources were provided by the NASA Columbia Supercomputer.

References

Albert, J. M. (1994), Quasi-linear pitch angle diffusion coefficients: Retaining high harmonics, *J. Geophys. Res.*, *99*, 23,741–23,745.

Borovsky, J. E., et al. (1997), The superdense plasma sheet: Plasmaspheric origin, solar wind origin, or ionospheric origin?, *J. Geophys. Res.*, *102*, 22,089–22,097.

Chen, M. W., L. R. Lyons, and M. Schulz (1994), Simulations of phase space distributions of storm time proton ring current, *J. Geophys. Res.*, *99*, 5745–5759.

Chen, M. W., S. Liu, M. Schulz, J. L. Roeder, and L. R. Lyons (2006), Magnetically self-consistent ring current simulations during the 19 October 1998 storm, *J. Geophys. Res.*, *111*, A11S15, doi:10.1029/2006JA011620.

Denton, M. H., M. F. Thomsen, H. Korth, S. Lynch, J. C. Zhang, and M. W. Liemohn (2005), Bulk plasma properties at geosynchronous orbit, *J. Geophys. Res.*, *110*, A07223, doi:10.1029/2004JA010861.

Ebihara, Y., and M. Ejiri (2000), Simulation study on fundamental properties of the storm-time ring current, *J. Geophys. Res.*, *105*, 15,843–15,859.

Freeman, J. W., et al. (1993), Magnetospheric specification model development code documentation, scientific description, and software documentation, contract F19628-90-K-0012, Rice Univ. for Air Force Geophys. Lab., Hanscom, AFB, Mass.

Korth, H., M. F. Thomsen, J. E. Borovsky, and D. J. McComas (1999), Plasma sheet access to geosynchronous orbit, *J. Geophys. Res.*, *104*, 25,047–25,061.

Kozyra, J. U., V. K. Jordanova, J. E. Borovsky, M. F. Thomsen, D. J. Knipp, D. S. Evans, D. J. McComas, and T. E. Cayton (1998), Effects of a high-density plasma sheet on ring current development during the November 2–6, 1993, magnetic storm, *J. Geophys. Res.*, *103*, 26,285–26,306.

Lavraud, B., and V. K. Jordanova (2007), Modeling the effects of cold-dense and hot-tenuous plasma sheet on proton ring current energy and peak location, *Geophys. Res. Lett.*, *34*, L02102, doi:10.1029/2006GL027566.

Lavraud, B., et al. (2005), Superposed epoch analysis of dense plasma access to geosynchronous orbit, *Ann. Geophys.*, *23*(7), 2519–2529.

Lavraud, B., M. F. Thomsen, J. E. Borovsky, M. H. Denton, and T. I. Pulkkinen (2006), Magnetosphere preconditioning under northward IMF: Evidence from the study of coronal mass ejection and corotating interaction region geoeffectiveness, *J. Geophys. Res.*, *111*, A09208, doi:10.1029/2005JA011566.

Liemohn, M. W., J. U. Kozyra, M. F. Thomsen, J. L. Roeder, G. Lu, J. E. Borovsky, and T. E. Cayton (2001), Dominant role of the asymmetric ring current in producing the stormtime *Dst**, *J. Geophys. Res.*, *106*, 10,883–10,904.

Liu, S., M. W. Chen, M. Schulz, and L. R. Lyons (2006), Initial simulation results of storm-time ring current in a self-consistent magnetic field model, *J. Geophys. Res.*, *111*, A04225, doi:10.1029/2005JA011194.

Lyons, L. R. (1974), Electron diffusion driven by magnetospheric electrostatic waves, *J. Geophys. Res.*, *79*, 575–580.

Stern, D. (1974), Models of the Earth's electric field, *Rep. X-602-74-159*, NASA Goddard Space Flight Cent., Greenbelt, Md.

Thomsen, M. F., J. E. Borovsky, R. M. Skoug, and C. W. Smith (2003), Delivery of cold, dense plasma sheet material into the near-Earth region, *J. Geophys. Res.*, *108*(A4), 1151, doi:10.1029/2002JA009544.

Tsyganenko, N. A. (1996), Effects of the solar wind conditions on the global magnetospheric configuration as deduced from data-based field models, *Eur. Space Agency Spec. Publ.*, *ESA SP 389*, 181–185.

Volland, H. (1973), A semiempirical model of large-scale magnetospheric electric fields, *J. Geophys. Res.*, *78*, 171–180.

Wang, C.-P., L. R. Lyons, M. W. Chen, R. A. Wolf, and F. R. Toffoletto (2003), Modeling the inner plasma sheet protons and magnetic field under enhanced convection, *J. Geophys. Res.*, *108*(A2), 1074, doi:10.1029/2002JA009620.

Wolf, R. A. (1983), The quasi-static (slow-flow) region of the magnetosphere, in *Solar Terrestrial Physics*, edited by R. L. Carovillano and J. M. Forbes, pp. 303–368, D. Reidel, Norwell, Mass.

M. W. Chen, Aerospace Corporation, M2-260, El Segundo, CA 90245, USA. (mchen@aero.org)

L. R. Lyons and C.-P. Wang, Department of Atmospheric and Oceanic Sciences, University of California, Los Angeles, 405 Hilgard Avenue, Los Angeles, CA 90095, USA.

M. Schulz, Lockheed Martin Advanced Technology Center, Palo Alto, CA 94304, USA.